

The Nature of the Velocity Field in Molecular Clouds. I. The Non-Magnetic Case

Enrique Vázquez-Semadeni¹ ^{*}, Ricardo F. González¹ [†], Javier Ballesteros-Paredes¹ [‡],
Adriana Gazol¹ [§], and Jongsoo Kim² [¶]

¹ Centro de Radioastronomía y Astrofísica, Universidad Nacional Autónoma de México, Apdo. Postal 3-72, Morelia, 58089, México

² Korea Astronomy and Space Science Institute, 61-1, Hwaam-dong, Yuseong-gu, Daejeon 305-764, Korea

8 November 2021

ABSTRACT

We present numerical simulations designed to test some of the hypotheses and predictions of recent models of star formation. We consider a set of three numerical simulations of randomly driven, isothermal, non-magnetic, self-gravitating turbulence with different rms Mach numbers M_s and physical sizes L , but with approximately the same value of the virial parameter, $\alpha \approx 1.2$. We obtain the following results: a) We test the hypothesis that the collapsing centers originate from locally Jeans-unstable (“super-Jeans”), subsonic fragments; we find no such structures in our simulations, suggesting that collapsing centers can arise also from regions that have supersonic velocity dispersions but are nevertheless gravitationally unstable. b) We find that the fraction of small-scale super-Jeans structures is larger in the presence of self-gravity. c) There exists a trend towards more negative values of the velocity field’s mean divergence in regions with higher densities, implying the presence of organized inflow motions within the structures analysed. d) The density probability density function (PDF) deviates from a lognormal in the presence of self-gravity, developing an approximate power-law high-density tail, in agreement with previous results. e) Turbulence alone in the large-scale simulation ($L = 9$ pc) does not produce regions with the same size and mean density as those of the small-scale simulation ($L = 1$ pc). Items (b)-(e) suggest that self-gravity is not only involved in causing the collapse of Jeans-unstable density fluctuations produced by the turbulence, but also in their *formation*.

We then measure the “star formation rate per free-fall time”, SFR_{ff} , as a function of M_s for the three runs, and compare with the predictions of recent semi-analytical models. We find marginal agreement to within the uncertainties of the measurements. However, within the $L = 9$ pc simulation, subregions with similar density and size to those of the $L = 1$ pc simulation differ qualitatively from the latter in that they exhibit a global convergence of the velocity field $\nabla \cdot \mathbf{v} \sim -0.6 \text{ km s}^{-1} \text{ pc}^{-1}$ on average. This suggests that the assumption that turbulence in clouds and clumps is purely random is incomplete. We conclude that a) part of the observed velocity dispersion in clumps must arise from clump-scale inwards motions, even in driven-turbulence situations, and b) analytical models of clump and star formation need to take into account this dynamical connection with the external flow and the fact that, in the presence of self-gravity, the density PDF may deviate from a lognormal.

Key words: interstellar matter – stars: formation – turbulence

1 INTRODUCTION

The role of the velocity field in the process of star formation (SF) remains not fully understood. It is generally believed nowadays that supersonic turbulent motions of a given size scale in molecular clouds (MCs)

^{*} E-mail: e.vazquez@astrosmo.unam.mx

[†] E-mail: rf.gonzalez@astrosmo.unam.mx

[‡] E-mail: j.ballesteros@astrosmo.unam.mx

[§] E-mail: a.gazol@astrosmo.unam.mx

[¶] E-mail: jskim@kasi.re.kr

should have a dual role in relation to SF (e.g., Sasao 1973; Ballesteros-Paredes, Vázquez-Semadeni, & Scalo 1999; Vázquez-Semadeni & Passot 1999; Klessen, Heitsch & Mac Low 2000; McKee & Ostriker 2007): they are thought to provide support towards scales larger than their own, while simultaneously promoting collapse of smaller scales. However, the origin and nature of the observed supersonic motions remains controversial. More than three decades ago, Goldreich & Kwan (1974) suggested that the observed supersonic widths of various molecular lines could be representative of gravitational contraction, although this suggestion was dismissed shortly thereafter by Zuckerman & Palmer (1974) through the argument that if all MCs were collapsing and converting most of their mass into stars in roughly one free-fall time, the resulting star formation rate would be at least 10 times larger than that presently observed in the Galaxy. Zuckerman & Evans (1974) then proposed that the supersonic linewidths in the clouds are produced primarily by local, small-scale motions, a scenario to which we refer as “local turbulence”, and which has been widely accepted until recently. Built into this scenario is the notion that local turbulence acts as a sort of isotropic pressure, so that it provides an important (and perhaps dominant) contribution in the support of the clouds against their self-gravity, in particular allowing for a state of near hydrostatic equilibrium (e.g., McKee & Tan 2003; Hennebelle & Chabrier 2008; Field, Blackman, & Keto 2008).

However, this scenario faces a number of problems. First, it is well known (e.g., Frisch 1995) that turbulent flows possess the largest velocity differences at the largest scales, a property which implies that the largest velocity differences within a turbulent structure are expected to occur at scales comparable to the size of the structure itself. That is, Lagrangian (i.e., moving with the flow) clumps are expected to be continually distorted (sheared and/or compressed) by these large-scale motions, in contradiction with the idea of their being in near equilibrium (Ballesteros-Paredes, Vázquez-Semadeni, & Scalo 1999). Such large-scale motions are indeed observed in molecular clouds and their substructure (e.g., Brunt 2002; Ossenkopf & Mac Low 2002; Heyer & Brunt 2007).

Second, there is the problem of how to maintain the observed turbulence levels. Early suggestions were that the turbulent motions consisted of hydromagnetic waves (e.g., Arons & Max 1975; Mouschovias 1976; Shu, Adams & Lizano 1987), which would be less dissipative than supersonic hydrodynamic turbulence. However, numerical experiments demonstrated that MHD turbulence generally decays as fast as hydrodynamic turbulence (Stone, Ostriker & Gammie 1998; Mac Low 1999; Padoan & Nordlund 1999), except perhaps if it is unbalanced (i.e., if the energy flux along field lines in one direction differs from that in the opposite direction; Cho, Lazarian & Vishniac 2002), although it is not clear whether this applies to MCs.

Maintenance of the turbulence in MCs by stellar energy feedback has also been proposed, although it is not yet clear whether this feedback can keep the clouds near equilibrium (e.g., Norman & Silk 1980; McKee 1989; Matzner & McKee 2000; Krumholz, Matzner, & McKee 2006; Nakamura & Li 2007) or rather disrupt them (e.g., Whitworth 1979;

Larson 1987; Franco, Shore & Tenorio-Tagle 1994; Hartmann, Ballesteros-Paredes & Bergin 2001). In both cases, the stellar feedback has been proposed as a regulating mechanism of the star formation efficiency (SFE). In the former, because the high stationary turbulence levels are expected to maintain the star formation rate (SFR) at low values (e.g., Klessen, Heitsch & Mac Low 2000; Heitsch, Mac Low & Klessen 2001; Vázquez-Semadeni et al. 2003, 2005b; Nakamura & Li 2007), while in the latter the SFR can be large after a cloud forms, but the cloud is soon dispersed after SF begins. Indeed, clusters over 5-10 Myr old are generally observed to be devoid of molecular gas (e.g., Leisawitz, Bash, & Thaddeus 1989; Hartmann, Ballesteros-Paredes & Bergin 2001; Ballesteros-Paredes & Hartmann 2007).

Another alternative that has been proposed recently is that MCs obtain their turbulence from the compressions that form them in the first place through various instabilities (Koyama & Inutsuka 2002; Vázquez-Semadeni et al. 2003; Audit & Hennebelle 2005; Heitsch et al. 2005, 2006; Vázquez-Semadeni et al. 2006), although in this case the turbulence should begin to decay after the compression that formed the cloud subsides. Vázquez-Semadeni et al. (2007) showed simulations in which, when this happens, the cloud begins to contract gravitationally, exhibiting a virial-like energy balance $|E_{\text{grav}}| \sim 2E_{\text{kin}}$ while doing so, even though the cloud is never in virial equilibrium. This can in fact be understood because, in the case of gravitational collapse, the velocity dispersion is at most within a factor of $\sqrt{2}$ from the value needed for equipartition. Thus, both a system in virial equilibrium and one in free-fall are, to order of magnitude, in energy equipartition, and are, thus, observationally indistinguishable on the basis of velocity dispersion alone (Ballesteros-Paredes 2006).

If the simulations by Vázquez-Semadeni et al. (2007) are representative of actual MCs, the nonthermal motions in the clouds could transit from being initially due to actual random turbulence, to later being due to gravitational contraction. In this case, the pseudo-virial energy balance would be a manifestation of the gravitational contraction rather than of virial equilibrium. We refer to this mode of flow, in which the velocity field at all scales contains a significant inflow component, as *large-scale inflow (LSI)*. Such a flow can be due to either generic dynamic compressions in the ISM (e.g., expanding HII regions or supernova remnants, or the transonic turbulence in the warm ISM), or to various large-scale instabilities, such as gravitational or magneto-Jeans (e.g., Li, Mac Low & Klessen 2005; Kim & Ostriker 2006, see also the review by Hennebelle, Mac Low & Vázquez-Semadeni 2008).

The scenario of LSI driven by self-gravity is actually frequently encountered. Since it is standard in simulations of star formation in clouds with decaying turbulence (e.g., Bate, Bonnell, & Bromm 2003; Bonnell & Bate 2006), it is often associated with a regime of decaying turbulence, although in principle there is no reason why it should be only applicable in this case. Field, Blackman, & Keto (2008) have attempted to describe a gravitationally-driven mass cascade that involves the formation of smaller-scale structures by gravitational contraction of larger-scale ones, followed by virialization at the small scales. The LSI scenario is also consistent with a number of recent studies suggest-

ing that indeed some MCs (Hartmann & Burkert 2006) and clumps (Peretto, Hennebelle & André 2007) may be undergoing global gravitational contraction. It should be noted, however, that the simulations supporting this scenario have generally been non-magnetic, possibly biasing the results. Elmegreen (2007) has recently suggested that clouds may collapse in regions where they are magnetically supercritical, while their subcritical fragments may remain supported for times significantly longer than their free-fall time.

One fundamental distinction between the hypotheses of local turbulence and of LSI is that, in the former, the kinetic energy of the turbulent motions internal to a clump is assumed to act fully as support against gravity, while in the latter, part of the kinetic energy of these motions may be globally compressive, either promoting collapse or being a consequence of it (Hunter & Fleck 1982; Ballesteros-Paredes, Vázquez-Semadeni, & Scalo 1999; Ballesteros-Paredes 2006; Dib et al. 2007). Recent models of the SFR (e.g., Elmegreen 2002; Krumholz & McKee 2005) or of the turbulent clump mass function as the origin of the stellar initial mass function (Padoan & Nordlund 2002; Hennebelle & Chabrier 2008) have been formulated under the assumption of local turbulence. It is thus important to determine whether this assumption is verified in numerical simulations of self-gravitating turbulence. The realization of the LSI scenario would thus imply a reduced amount of support against self-gravity.

Moreover, the models by Padoan & Nordlund (2002, hereafter PN02), Elmegreen (2002) and Krumholz & McKee (2005, hereafter KM05) rely on the idea advanced by Padoan (1995), Elmegreen (2002) and Vázquez-Semadeni et al. (2003) that the mass that proceeds to collapse is that which is deposited by the turbulence in subsonic, yet Jeans-unstable (“super-Jeans”) fragments. The latter authors provided indirect evidence that this could be so by showing the existence of a correlation between the SFE and the so called “sonic scale” of the turbulence, the scale below which the turbulent motions are subsonic on average. However, it is not necessary that *only* the mass in these subsonic, super-Jeans structures proceeds to collapse. Material in supersonic, yet effectively gravitationally unstable structures can also participate in the collapse.

The goal of the present paper is to contribute towards the understanding of the role of the velocity field’s topology on the control of the star formation process. To this end, we use numerical simulations (described in §2) of randomly driven turbulence in isothermal, self-gravitating flows aimed at investigating whether the hypotheses and predictions of analytical models are verified in the non-magnetic case. The simulations have different sizes, mean densities and velocity dispersions, but scaled so that all have approximately the same value of the virial parameter $\alpha \equiv 2E_{\text{kin}}/|E_{\text{grav}}|$, thus satisfying the hypotheses of the KM05 model. In these simulations, we first search for the fraction of super-Jeans, subsonic subregions in a cloud, to see whether they can be deemed responsible for the mass that ends up collapsing (§3). Second, we investigate whether the internal velocity dispersion in dense subregions of a cloud can be considered as random as that at larger scales (§4), or instead exhibits increasing amounts of the compressive component as the density of the structures increases and their size decreases. In §5, we ask whether the suite of simulations agrees with

the prediction of the model by KM05 for the dependence of the SFR_{ff} on the turbulent Mach number. Finally, in §6 we summarize and discuss the implications of our results, in particular comparing with previous work.

2 THE MODELS

We have performed three simulations of non-magnetic, self-gravitating, isothermal turbulence at a resolution of 512^3 zones, using a total variation diminishing (TVD) scheme (Kim et al. 1999) with periodic boundaries and random Fourier driving with a spectrum $P(k) = k^6 \exp(-8k/k_{\text{pk}})$. Here, k is the wavenumber and $k_{\text{pk}} = 2(2\pi/L)$ is the energy-injection wavenumber, with L being the computational box size. The energy is thus injected mostly at scales of order half the box size. The driving is purely rotational (or “solenoidal”), thus having no compressive component. A prescribed rate of energy injection is applied in order to approximately maintain the rms Mach number $M_s \equiv \sigma/c_s$ near a “nominal” value that characterizes the run. Here, σ is the three-dimensional velocity dispersion and c_s is the sound speed, taken equal to 0.2 km s^{-1} in all runs (corresponding to $T = 11.4 \text{ K}$). The actual value of M_s fluctuates and is slightly different from the nominal value, because the numerical scheme is designed to maintain a constant energy injection rate, not a constant rms Mach number.

The other parameter that characterizes a simulation is the “Jeans number” $J \equiv L/L_J$, where $L_J \equiv (\pi c_s^2/G\rho)^{1/2}$ is the Jeans length, with $\rho \equiv \mu n_0$ being the mean density of the simulation, n_0 the mean number density, $\mu = 2.36 m_{\text{H}}$ the mean particle mass, and m_{H} the mass of the Hydrogen atom. All three simulations are evolved for 3.2 turbulent crossing times before turning on self-gravity, in order for the turbulence to reach a fully developed state, and thus avoid applying the self-gravity directly on the imprints of the random driving. The three simulations differ in physical size L , mean density n_0 and nominal rms Mach number M_s , but in each case their values are chosen as to give the same value of the ratio M_s/J . The nominal values of the pairs (M_s, J) for the three runs are (8, 2), (16, 4), and (24, 6), respectively, corresponding to a nominal value of $M_s/J = 4$. The runs are named mnemonically by means of their values of M_s and J .

Note that $(M_s/J)^2$ is proportional to the virial parameter α , as can be seen by approximating $E_{\text{kin}} \approx \mathcal{M}\sigma^2/2$, where \mathcal{M} is the total mass in the simulation, and $|E_{\text{grav}}| \approx G\mathcal{M}^2/L$. For a spherical cloud of mass $\mathcal{M} = 4\pi\rho L^3/3$, we thus have

$$\alpha \equiv \frac{2E_{\text{kin}}}{|E_{\text{grav}}|} \approx \frac{\mathcal{M}\sigma^2}{G\mathcal{M}^2/L} = \frac{3}{4\pi^2} \frac{M_s^2}{J^2}. \quad (1)$$

Our simulations thus all have a nominal value of $\alpha \approx 1.22$. The actual average values of M_s and of α , together with other parameters of the runs, are indicated in Table 2, in which the column labeled t_{grav} gives the time at which self-gravity is turned on, and the column labeled “ M_s (real)” gives the actual measured average value of the rms Mach number over the duration of the run.

It is also worth noting that fixing the ratio M_s/J only fixes the ratio $\sigma/(\rho^{1/2}L)$ (at a given c_s), and so we still have freedom to choose the values of the individual physical pa-

RUN PARAMETERS

Name	L [pc]	n_0 [cm^{-3}]	M [M_\odot]	L_J [pc]	J	M_s (real)	α (real)	v_{rms} [km s^{-1}]	t_{ff} [Myr]	t_{grav} [Myr]	t_{turb} (nominal) [Myr]	grid cell size [pc]
Ms8J2	1	2000	115.8	0.5	2	8.6	1.4	1.7	2.5	2	0.625	0.00195
Ms16J4	4	500	1853	1	4	15.7	1.2	3.1	5	4	1.25	0.00781
Ms24J6	9	222.22	9382	1.5	6	23.0	1.1	4.6	7.5	6	1.875	0.0175

rameters. We do this by assuming that the size L and mean density n_0 of our simulations satisfy one of Larson’s (1981) relations, i.e., $n_0 \propto L^{-1}$. Since all three simulations have the same nominal value of α , then the above assumption also implies that our suite of simulations also satisfies the other Larson relation, $\sigma \propto L^{1/2}$. The set of physical values for the simulations are also reported in Table 2.

3 FRACTION OF SUBSONIC, SUPER-JEANS STRUCTURES

3.1 Procedure

In this section, we measure, as a function of region size, the fraction of regions in the numerical simulations that is both subsonic and super-Jeans, in order to test the hypothesis that these are indeed the structures that collapse gravitationally to form stars. For generality, we consider two types of regions: a) the set of all cubic sub-boxes of a simulation of a given size and b) dense clumps defined by a density threshold criterion. The first set contains both overdense and underdense regions, and is intended to provide unbiased statistics of the velocity field in all subregions of a given size within the numerical box, independently of the local density. The second set contains only overdense clumps.

To isolate the effect of self-gravity, we perform the procedure at two different times in each simulation. First, we consider the last data dump before gravity is turned on, at which the density distribution must be a consequence of the turbulent flow alone. Second, we consider a data dump at around two free-fall times t_{ff} after having turned gravity on, at which significant gravitational collapse has occurred, and the density structure should be the result of the combined effects of turbulence and self-gravity.

For the analysis using sub-boxes of the simulation, we subdivide the latter in cubic sub-boxes of sizes 2, 4, 8, 16, 32, 64, and 128 grid zones per dimension. Since the simulations are performed at a resolution of 512 grid cells per dimension, and runs Ms8J2, Ms16J4 and Ms24J6 respectively have sizes $L = 1, 4$ and 9 pc, the grid cell size differs for each run, and is also indicated in Table 2. It should be noted that, since the sub-boxes are located at fixed positions within the simulation box, their locations bear no special relation with those of actual clumps. A clump may be located at the interface between two sub-boxes, and it in general moves from one sub-box to another as time elapses. However, we make no attempt to repeat the procedure shifting the positions of the sub-boxes to find a possible “best” match between the sub-

boxes and the actual clumps. We consider that the number of sub-boxes is large enough that no particular choice of the origins of the boxes is better than any other.

For the analysis with clumps, we define a clump as a connected set of grid cells with densities above a certain threshold. To create an ensemble of clumps, we consider a series of thresholds, of $n = 32, 64, 128$ and 256 times the mean density of the simulation. We then approximate their size by $L = (3V/4\pi)^{1/3}$, where V is their volume. As discussed by Vázquez-Semadeni et al. (2005a), this is a rather robust estimator of the clumps’ size. Finally, for the plots, the clumps are classified by their sizes (independently of the threshold from which they originated) and added to logarithmic size bins defined by successive powers of 2 from 2 to 64 grid cells.

For each region (sub-box or clump), we compute its mean density, its internal three-dimensional velocity dispersion σ^2 (subtracting the region’s mean velocity), and whether it is Jeans stable or unstable. In the case of sub-boxes, since their size is predetermined and the temperature is constant in space and time, we simply compute the critical density for Jeans instability (i.e., with respect to thermal support only)¹ at the specified size. Since the flow is isothermal, this “Jeans density” is unique at a given scale, and thus we can compare it with the sub-box’s mean density. For the clumps, we simply compare their estimated size to the Jeans length derived from the clump’s mean density. Finally, we count the number of regions that have a size larger than their associated Jeans length, the number of regions that have a subsonic velocity dispersion, and the number of regions that satisfy both conditions simultaneously.

Note also that, in the case of clumps, we have not corrected for the possibility of them being located at the boundaries of the periodic numerical box. So, if a clump crosses one or more boundaries, it is artificially split into two or more fragments by our clump-defining algorithm. However, we do not expect this minor omission to introduce any serious biases since, as we discuss in §3.2, the fraction of super-Jeans clumps is found to already be unity at the largest sizes (clumps of even larger size would be even more super-Jeans), and the fraction of subsonic clumps is already zero at scales significantly smaller than the largest clump sizes

¹ We do not consider the non-thermal contribution to the “support”, since we are only interested in the fraction of simultaneously subsonic and super-Jeans structures. Moreover, as discussed in §4, it is not clear that all of the non-thermal kinetic energy can be considered to provide support.

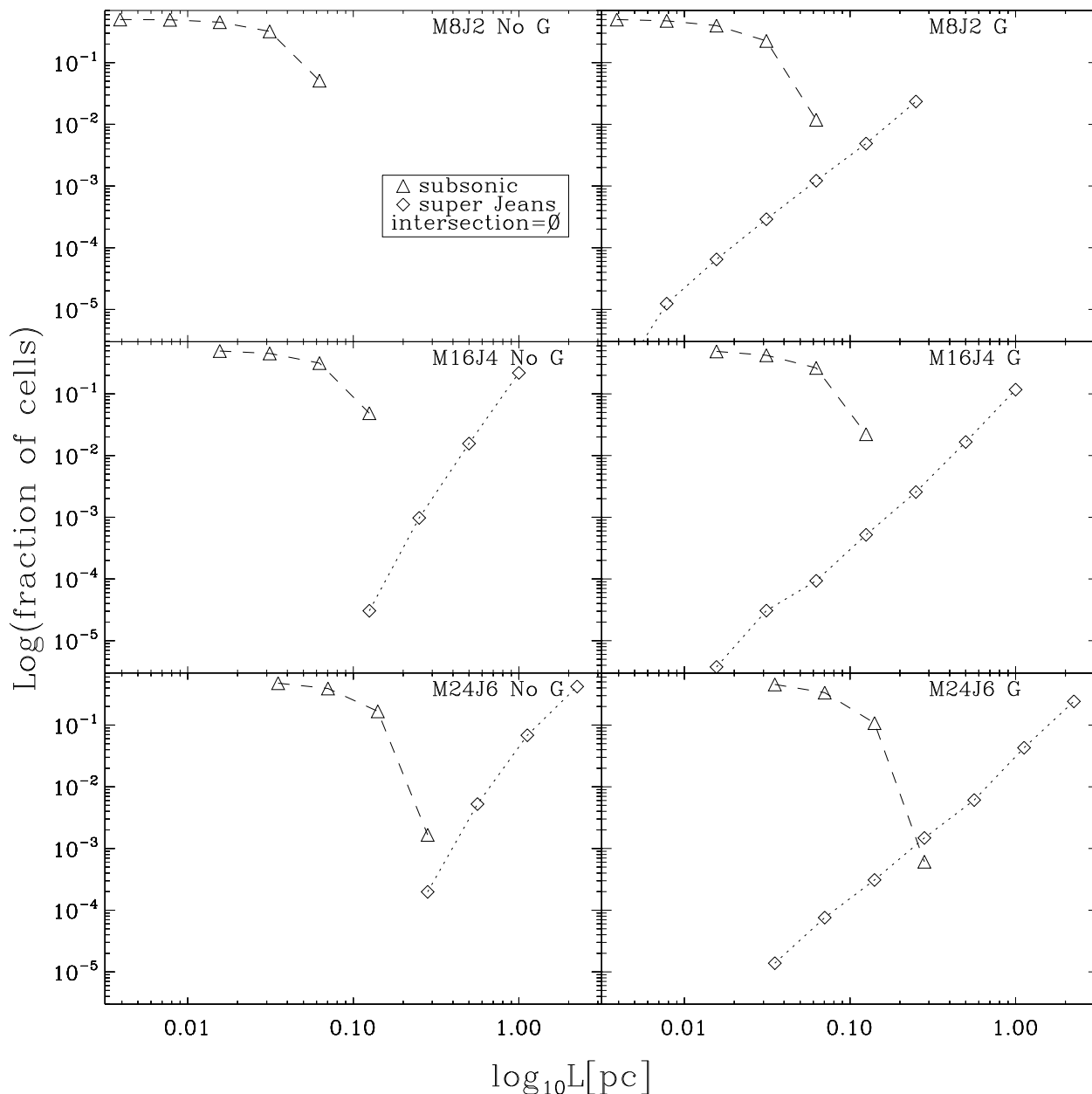


Figure 1. Fraction of subsonic (*triangles, dotted lines*) and of super-Jeans (*diamonds, solid lines*) sub-boxes in runs Ms8J2 (*top row*), Ms16J4 (*middle row*), and Ms24J6 (*bottom row*), as a function of sub-box size. The entire numerical box is subdivided in sub-boxes of the indicated size. The *left* panels show the fractions shortly before the time when self-gravity is turned on (t_{grav}). The *right* panels show the fractions at approximately two free-fall times after t_{grav} . The fraction of sub-boxes that are both subsonic and super-Jeans is zero at all sub-box sizes, and thus cannot be shown in this figure.

found (clumps of larger size would be expected to be even more supersonic). Besides, the sizes of the clumps are never larger than 1/10th of the numerical box, and so the probability of them crossing the boundary is relatively low.

3.2 Results

The fractions of subsonic and super-Jeans structures for the three runs are shown for sub-boxes in Fig. 1 and for clumps

in Fig. 2. In both figures, the *top row* shows results for run Ms8J2, the *middle row* shows run Ms16J4, and the *bottom row* shows run Ms24J6; the *left* panels show the result before the time at which self-gravity is turned on (t_{grav} ; cf. Table 2), and the *right* panels show it at approximately two free-fall times after t_{grav} . Note that, for the sub-boxes, the fractions can be very small, and are thus shown in logarithmic scale.

The most notable result of this analysis is that *the set of simultaneously subsonic and super-Jeans structures (ei-*

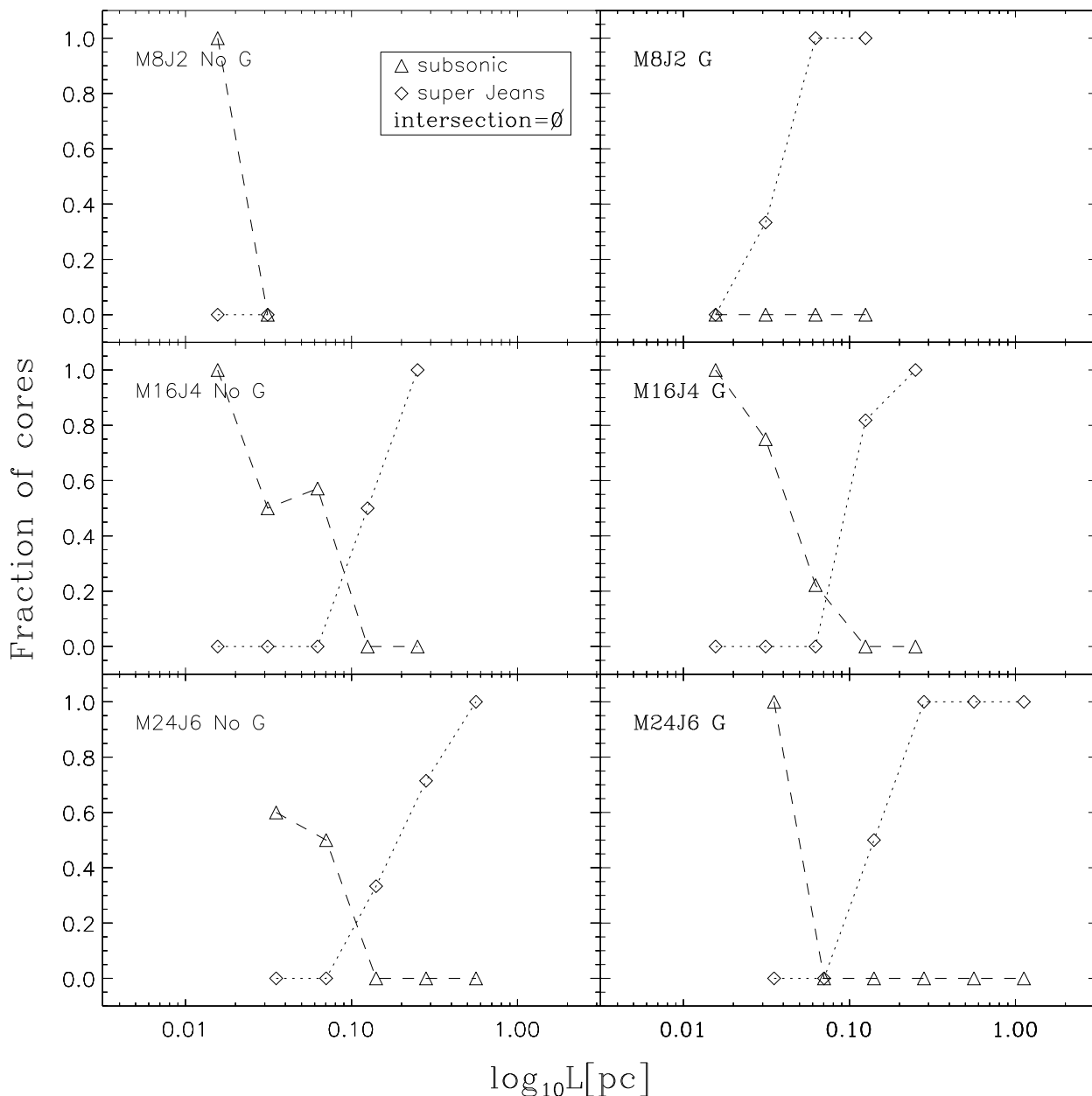


Figure 2. Same as Figure 1 but for clumps rather than sub-boxes. The clumps are defined as connected structures with densities above a density threshold. The ensemble of clumps was created by considering thresholds 32, 64, 128 and 256 times the mean density n_0 . The fraction of clumps that are both subsonic and super-Jeans is again zero at all clump sizes considered (not shown). Scales at which there are no clumps have no points drawn.

ther sub-boxes or clumps) is empty at all the scale sizes we sampled. Thus, this fraction is *not* plotted in Figures 1 and 2. We discuss the implications and limitations of this result in §6.

Some other features are worth noting. The fraction of subsonic (triangles, dotted lines) sub-boxes or clumps as a function of size shows no clear trend with the inclusion of self-gravity. However, the fraction of super-Jeans (diamonds, solid lines) structures at small (for sub-boxes) or intermediate (for clumps) scales tends to increase in the presence of

self-gravity. In fact, for the small-scale run Ms8J2 there are no super-Jeans sub-boxes in the absence of self-gravity, but significant amounts appear after it has been turned on. This means that *the presence of self-gravity changes the distribution of sub-box masses in comparison to that produced by turbulence alone, increasing the fraction of regions that can proceed to gravitational collapse.* That is, the effect of self-gravity can begin *prior* to the actual “capture” of a region to

proceed to collapse.² In other words, a density enhancement is in general expected to reach higher peak and mean densities in the presence of self-gravity than when it is produced only by turbulence. We refer to this as gravity aiding in the *production* of the density fluctuation, regardless of whether it eventually collapses or not.

This conclusion is also supported by the probability density function (PDF) for the density field of the three runs. In Fig. 3 we show the density PDFs of the three runs at 0, 1 and 2 times the global free-fall time, t_{ff} , of each simulation (cf. Table 2). The PDF at 0 t_{ff} is representative of the effects of turbulence alone, while those at 1 and 2 t_{ff} show the effect of turbulence and gravity combined. In all runs, the PDFs in the presence of self-gravity show a prominent high-density tail, implying that the relative frequency of high density regions is higher in this case, compared to the effect of turbulence alone. Similar results have been found by other workers (Klessen 2000; Dib & Burkert 2005). Thus, the *production* of super-Jeans structures is itself aided by the inclusion of self-gravity.

One final point to note is that, since higher density thresholds in general imply that the resulting clumps have smaller sizes and higher densities, the small clumps are generally also denser. Thus, Fig. 2 implies that there indeed exists a population of dense, subsonic clumps in the simulations, which, however, are not superJeans.

4 COMPRESSIVE COMPONENT OF THE VELOCITY FIELD IN DENSE STRUCTURES

We now investigate the nature of the velocity field in subregions of our turbulent supersonic flows, in particular aiming at whether our small-scale simulation Ms8J2 is statistically representative of regions of similar size within the large-scale run Ms24J6. For this purpose, we again subdivide the large-scale simulation’s (Ms24J6) domain into sub-boxes, but this time having the same size as the small-scale run Ms8J2. Note, however, that run Ms8J2 has a size of 1/9th that of run Ms24J6. Since the latter has a resolution of 512 grid cells per dimension, then the sub-boxes should span $512/9 = 56.89$ cells per dimension, which we round to 57 cells. Due to this rounding, we cannot fit 9 full, non-intersecting sub-boxes along each direction within the whole box, and thus we only consider the first 8 sub-boxes from the origin in each direction, for a total of $8^3 = 512$ sub-boxes, each with a linear size of 57 grid cells.

For each sub-box, we measure its mean density and the mean divergence of its velocity field. To compute the divergence, we Fourier-transform the three velocity components for the entire simulation box, and compute the divergence in Fourier space as

$$\mathcal{F}(\nabla \cdot \mathbf{v}) = -i\mathbf{k} \cdot \mathbf{v}_k, \quad (2)$$

where $i = \sqrt{-1}$, $\mathcal{F}()$ denotes the Fourier transform of its argument, \mathbf{k} is the wavevector, and \mathbf{v}_k is its associated

² We say that a certain density enhancement is “captured” by gravity when it was originally produced by a turbulent compression, but at some time while its mass and/or density are increasing, it suddenly becomes gravitationally unstable and begins to undergo gravitational collapse.

Fourier velocity amplitude. We then transform back to physical space to obtain the divergence field for the whole box, and finally we take the average of this field in each sub-box.

Figure 4 shows the result of this exercise, giving the mean divergence of each sub-box of run Ms24J6 as a function of its mean density at two times before self-gravity is turned on: at $t = 4$ Myr ($= 2.1 t_{\text{turb}}$, where $t_{\text{turb}} \equiv L/v_{\text{rms}} \approx 1.875$ Myr is the “nominal” turbulent crossing time; cf. Table 2) on the *left* panel, and at $t = 6$ Myr $= 3.2 t_{\text{turb}}$ on the *right* panel. The contours show the two-dimensional histogram of the points, and are drawn at levels 0.143, 0.286, 0.428, 0.571, 0.714 and 0.857 of the maximum. Figure 5 shows the corresponding plot at times in which self-gravity has been on for 1 t_{ff} (*left panel*) and 1.93 t_{ff} (*right panel*), where $t_{\text{ff}} \equiv L_J/c_s$ is the free-fall time. The vertical lines in both figures show the mean densities of runs Ms24J6 (*dotted line*) and Ms8J2 (*dashed line*).

In all cases, the contours are seen to have an elongated shape, indicating that, although with abundant scatter, a positive correlation exists between the mean value of $-\nabla \cdot \mathbf{v}$ (i.e., the velocity *convergence*) and the mean density of the sub-boxes. The contours are more elongated in the cases with self-gravity, for which we find an average fit of

$$\left[\frac{\nabla \cdot \mathbf{v}}{\text{km s}^{-1} \text{pc}^{-1}} \right] \approx -(0.45 \pm 0.05) \log_{10} \left[\frac{n}{222 \text{ cm}^{-3}} \right] - 0.13 \pm 0.03, \quad (3)$$

where the uncertainties in the slope and the intercept span the range of values we have encountered in the two cases sampled. The fit implies that, at the size and mean density of run Ms8J2, which is 9 times smaller and denser than run Ms24J6, a mean divergence of $\sim -0.6 \text{ km s}^{-1} \text{pc}^{-1}$ should be expected. Instead, run Ms8J2, which is driven by random forcing at its own scale in order to mimic the assumption of local turbulence, has zero mean divergence by construction. The trend of $\nabla \cdot \mathbf{v}$ with mean density observed in the sub-boxes of the large-scale simulation Ms24J6 suggests that *the LSI scenario* (cf. §1) *is verified in the density enhancements even in driven turbulence regimes*.

It is also noteworthy that the probability of producing sub-boxes of the same density and size as run Ms8J2 in run Ms24J6 is extremely low (1 case in 1024, since each plot contains 512 points) in the absence of self-gravity (Fig. 4). This probability increases substantially in the presence of self-gravity (13 cases in 1024). Thus, we conclude that *the formation of regions with the same size and density as those of run Ms8J2 within run Ms24J6 seems to require the presence of self-gravity*. This result further reinforces the conclusion from §3 that self-gravity intervenes in the *formation* of super-Jeans structures, and not only in their collapse.

It is interesting to compare the magnitude of the convergence seen in Figs. 4 and 5 with that of the vorticity, in order to get an idea of which type of motion (potential or solenoidal) dominates within the subregions of run Ms24J6. Again, we calculate the vorticity in Fourier space as

$$\mathcal{F}(\nabla \times \mathbf{v}) = -i\mathbf{k} \times \mathbf{v}_k, \quad (4)$$

and use a similar averaging procedure for the Ms8J2-sized sub-boxes of run Ms24J6 as for the divergence. Since the vorticity is a (pseudo-)vector, in Fig. 6 we plot the magnitude of the average vorticity in each sub-box. This is shown

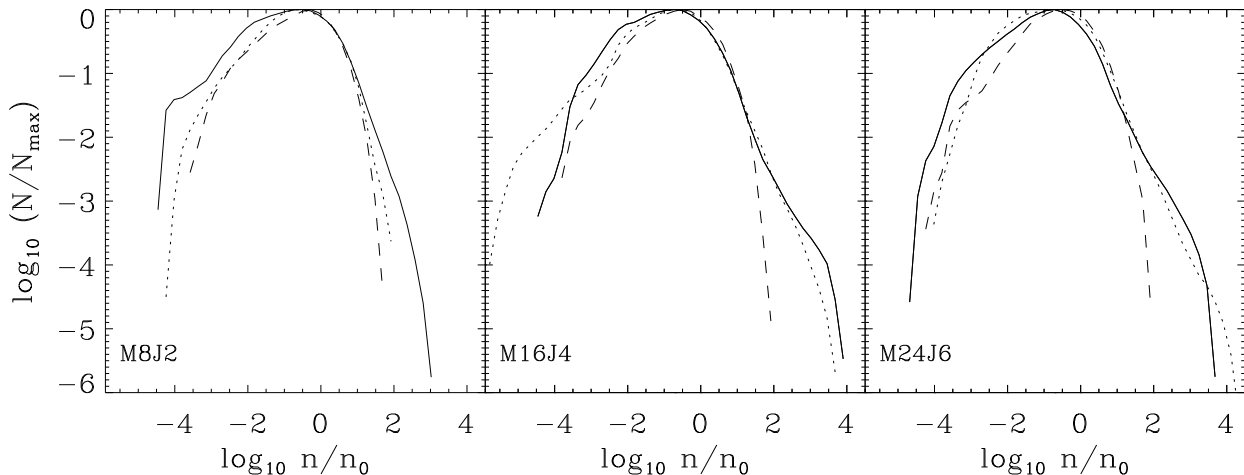


Figure 3. Probability density function (PDF) of the density field in the three runs at times $t = 0 t_{\text{ff}}$ (dashed line), $1 t_{\text{ff}}$ (dotted line), and $3 t_{\text{ff}}$ (solid line) after gravity was turned on, where t_{ff} is the global free-fall time of each simulation (cf. Table 2). The vertical axis is normalized to the number of grid cells at the maximum, N_{\max} .

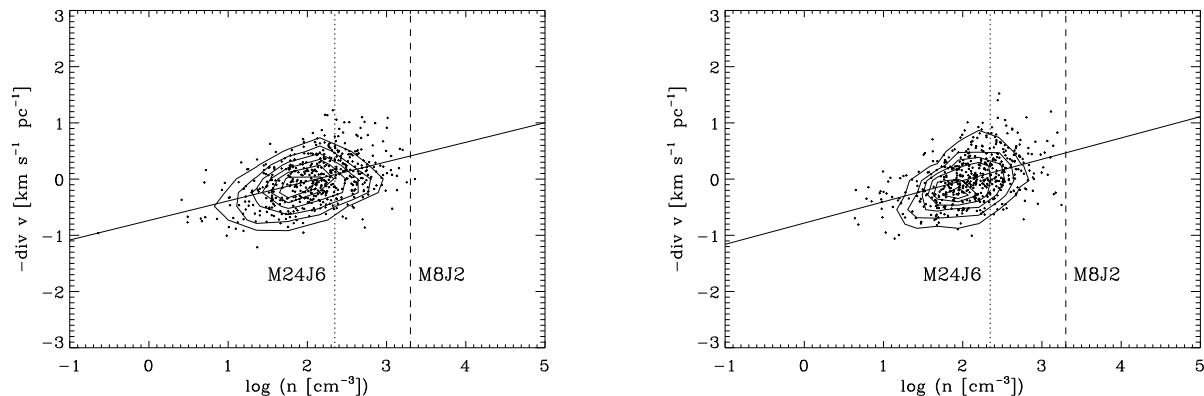


Figure 4. Negative mean divergence of the velocity field as a function of mean density for sub-boxes of the large-scale simulation Ms24J6 that have the same size as run Ms8J2, at two times without self-gravity: $t = 4$ Myr, corresponding to $2.1 t_{\text{turb}}$ into the evolution (left panel), and $t = 6$ Myr ($3.2 t_{\text{turb}}$; right panel), where t_{turb} is the turbulent crossing time of the simulation [run Ms24J6; see Table 2]). The straight solid lines show least-squares fits through the data points, and have slopes 0.35 (left panel) and 0.38 (right panel). The contours show the two-dimensional histogram of the distribution of points in the plot, at levels 0.143, 0.286, 0.429, 0.571, 0.714 and 0.857 of the maximum. The vertical lines show the mean density of simulations Ms24J6 (dotted line) and Ms8J2 (dashed line). It is seen that, in the absence of gravity, the formation of structures of the same size and mean density as those of run Ms8J2 is extremely unlikely within run Ms24J6.

at $t = 4$ Myr (a time without self-gravity; left panel) and at $t = 14$ Myr (a time with self-gravity; right panel). In general it is seen that the magnitudes of the divergence and of the vorticity are comparable, suggesting that the sub-boxes contain comparable amounts of the two types of motion.

Note, however, that it is not possible from these figures to obtain a quantitative estimate of the amount of kinetic energy contained in each type of motion, since, contrary to the case of the energies, not the divergence nor the vorticity nor their sum are bounded or conserved in any sense. It would be necessary to compare the kinetic energy in each type of motion directly but, because this task is not straightforward, we defer it to a future study. In any case, our simulations show that, to order of magnitude, the potential and solenoidal parts of the velocity gradient are comparable,

and therefore we expect the fraction of compressive energy present in dense regions to be substantial.

5 STAR FORMATION EFFICIENCY IN CONSTANT-VIRIAL-PARAMETER STRUCTURES

In this section we now proceed to measure the SFE in terms of what KM05 called the star formation rate per free-fall time, SFR_{ff} , in the three simulations, in order to test whether the predictions of their model are verified. Following KM05, we define the SFR_{ff} as the fraction of a cloud's mass that is deposited into stars in one free-fall time. As in previous papers (e.g., Vázquez-Semadeni et al. 2005b; Galván-Madrid et al. 2007), we approximate this fraction

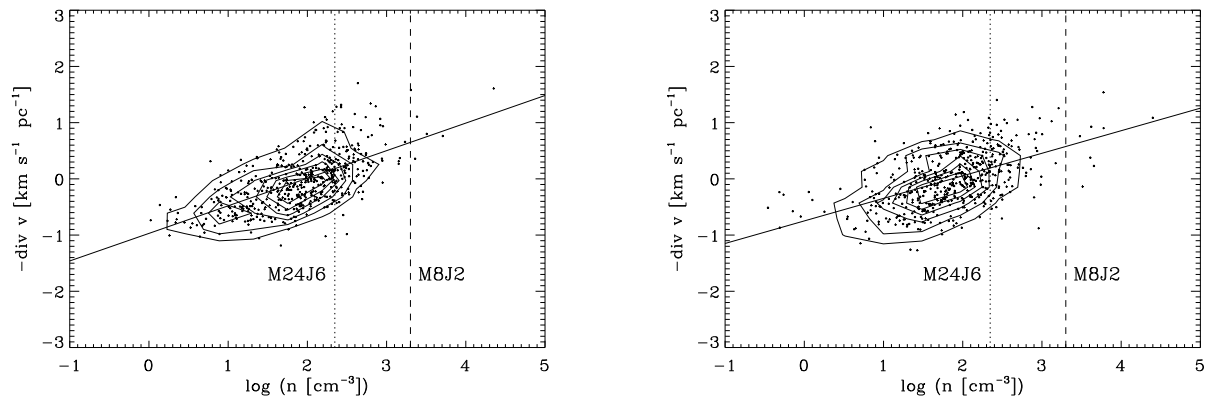


Figure 5. Same as Fig. 4 but at two times with self-gravity: $t = 14$ Myr (*left panel*) and $t = 20$ Myr (*right panel*) (respectively $1 t_{\text{ff}}$ and $1.93 t_{\text{ff}}$ after having turned on self-gravity, with t_{ff} being the global free-fall time of the simulation [run Ms24J6; see Table 2]). The slopes of the fits through the data points have slopes 0.50 (*left panel*) and 0.40 (*right panel*). We note that in the presence of self-gravity, the likelihood of forming structures with the same size as run Ms8J2 and mean density equal or larger than the mean density of the latter is significantly increased with respect to the case without self-gravity (Fig. 4).

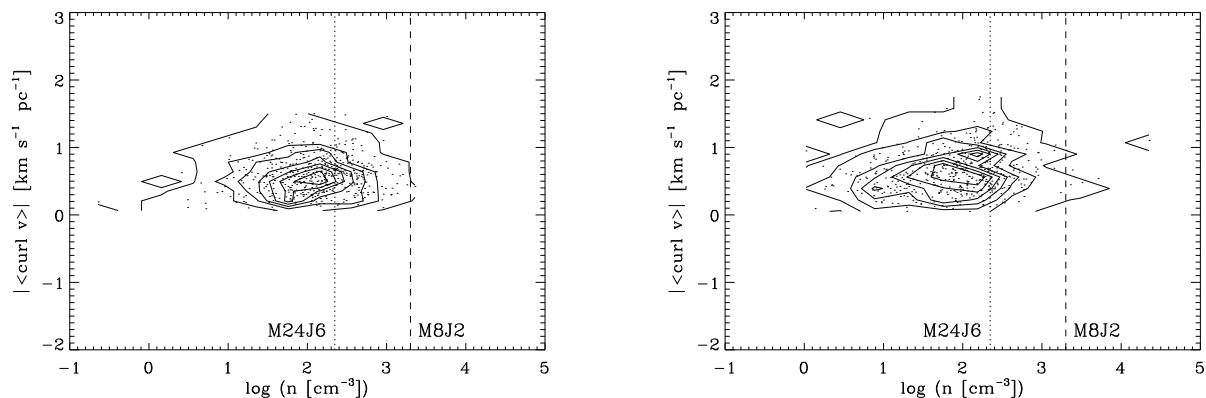


Figure 6. Same as Figs. 4 and 5, but for the magnitude of the vorticity at $t = 4$ Myr (*left panel*, without self-gravity) and $t = 14$ Myr (*right panel*, with self-gravity) (respectively, compare to the *left panels* of Figs. 4 and 5). It is seen that comparable magnitudes of the (negative) divergence and of the vorticity occur before and after turning self-gravity on.

as the fraction of the total mass in the simulation that is in regions with density above a certain threshold. The threshold is chosen to be unambiguously indicative that collapse has occurred. Specifically, we take a threshold density $n_{\text{thr}} = 1000 n_0$, which is a much larger density than can be achieved through the turbulent fluctuations alone in any of the runs, and guarantees that the mass contained in objects above those densities is either collapsing or gravitationally locked within them and does not redisperse (except for slight fluctuations, discussed in the next paragraph)³. As noted in Vázquez-Semadeni et al. (2005b), the collapsed (or “accreted”) mass fraction does not depend heavily on the chosen threshold, as long as the latter satisfies the above

³ Note that, in our simulations, gravitational collapse is necessarily terminated when most of the collapsed mass is deposited into a single or a few grid cells. It is in this sense that the material is “locked” into the collapsed objects, and by no means it should be interpreted as implying that a real hydrostatic object (other than one or several stars) has formed.

conditions. As a confirmation, we have also used a threshold $n_{\text{thr}} = 500 n_0$, and found no significant difference in the results, as described below. Note however that our procedure may overestimate the actual mass deposited into protostellar objects, since it assumes a 100% efficiency of conversion of gas into stars above the threshold density, while in actual cluster-forming cores, the expected efficiency is closer to 30-50% (Lada & Lada 2003).

The left panels of Figure 7 show the evolution of the mass accreted onto collapsed objects as a function of time after having turned gravity on, in units of Myr (*upper frame*) as well as in units of the free-fall time t_{ff} (*lower frame*). The SFR_{ff} is then the slope of the collapsed mass fraction versus time, the latter in units of t_{ff} .

The accretion histories of the runs are seen to be noisy, even exhibiting slight, occasional drops. This reflects the fact that our numerical scheme does not include any prescription for sink particles or cells, and therefore the mass in the collapsed object is not fully “locked” in the object – the outer parts of it may have densities that oscillate about

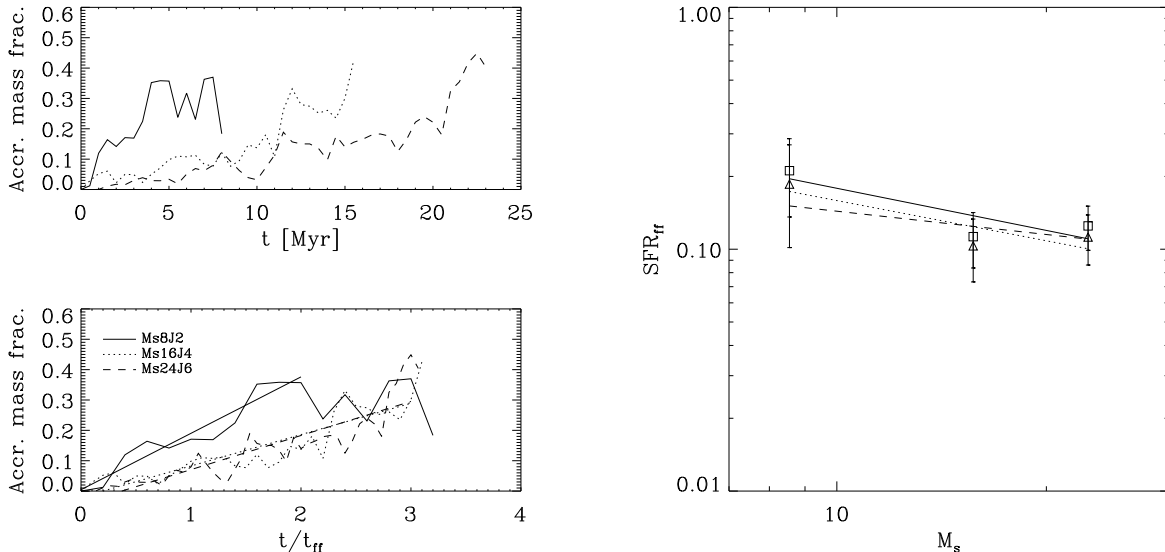


Figure 7. *Left panels:* Fraction of mass accreted onto collapsed objects as a function of time for the three simulations, with time in units of Myr (*top left*) and of the free-fall time of each simulation (*bottom left*). The average SFR_{ff} is computed by fitting a least-squares line to the plot of accreted mass vs. time-in-units-of- t_{ff} . *Right panel:* Star formation rate per free-fall time (SFR_{ff} , i.e., average accreted mass after one free-fall time) as a function of the time-averaged rms Mach number of the simulation for the three runs. *Triangles* (resp. *squares*) denote results obtained with a density threshold $n_{\text{thr}} = 1000 n_0$ (resp. $n_{\text{thr}} = 500 n_0$) for defining the collapsed objects. The *dotted* and *solid* lines show the best fits through the data points for $n_{\text{thr}} = 1000 n_0$ and $n_{\text{thr}} = 500 n_0$, respectively. The slope of the *dotted* line is -0.55 , while that of the *solid* line is -0.58 . The *dashed* line shows the prediction of the KM05 model, with slope -0.32 .

the threshold we use for defining the collapsed objects. This implies that the SFR_{ff} is determined only to within a certain uncertainty in our simulations. For estimating the average SFR_{ff} at each M_s , we thus fit a least-squares line to the plot of accreted mass vs. time (the latter in units of t_{ff} ; lower left panel of Fig. 7), and show error bars corresponding to $\pm 3\sigma$, where σ is the standard deviation of the fit. Note also that the accreted mass for run Ms8J2 appears to saturate at $t \sim 5 \text{ Myr} \sim 2t_{\text{ff}}$, so for this run we only take into account times shorter than this saturation time.

With this procedure, we obtain the average values of the SFR_{ff} shown in the *right panel* of Figure 7. For reference, we show the results obtained with the two thresholds $n_{\text{thr}} = 500 n_0$ and $n_{\text{thr}} = 1000 n_0$. We see that the data points are shifted slightly to higher values for the lower threshold, since the structures contain more mass, but the trend of the SFR_{ff} is essentially the same in both cases.

Our results can be compared with the prediction of the KM05 model, which those authors fitted by

$$\text{SFR}_{\text{ff}} \approx 0.014 \left(\frac{\alpha}{1.3} \right)^{-0.68} \left(\frac{M_s}{100} \right)^{-0.32}. \quad (5)$$

Thus, a residual dependence on the Mach number $\sim M_s^{-0.32}$ is expected in the KM05 model even at constant α . The slope of -0.32 is indicated in the *right panel* of Figure 7 by the *dashed* line, while the *solid* and *dotted* lines indicate fits to our data, with slopes -0.58 for $n_{\text{thr}} = 500 n_0$ and -0.55 for $n_{\text{thr}} = 1000 n_0$, respectively.

We see that, within the uncertainties, our results can accommodate the slope predicted by KM05, although the agreement is only marginal, because the most probable slope that we measure is significantly steeper than theirs. Besides, the

intercept of the fitted line appears to imply a larger coefficient than the one in eq. (5). For example, at $M_s = 10$, the *dotted* line ($n_{\text{thr}} = 1000 n_0$) in the right panel of Fig. 7 gives $\text{SFR}_{\text{ff}} \approx 0.15$, while eq. (5), with $\alpha = 1.2$, predicts $\text{SFR}_{\text{ff}} = 0.031$.

Several effects, both physical and of procedure, can account for these differences. Possible effects of procedure are: a) We are assuming a 100% efficiency of conversion from gas to stars above the density threshold. Instead, this efficiency is known to be $\sim 30\%$ for high-mass star forming cores (Lada & Lada 2003) and even lower for low-mass ones, so we are clearly overestimating the total mass deposited into stars by a factor of 3-10.⁴ b) KM05 calibrated their model using linear approximations to the SFEs of Vázquez-Semadeni et al. (2003), while in reality the mass accretion histories presented by those authors are strongly nonlinear. c) We have defined the free-fall time simply as $t_{\text{ff}} = L_J/c_s$, which is larger by a factor of $\sqrt{32/3\pi}$ than the alternate definition $t'_{\text{ff}} \equiv (3\pi/32G\rho)^{1/2}$. Our choice is a reasonable estimate, since actual collapse appears to take

⁴ Note that, because we use a threshold that is simply a fixed multiple of the simulation's mean density, we may be biasing the measured slope, since the *physical* threshold density is highest in the small-scale run Ms8J2 and lowest in the large-scale one, Ms24J6. However, correcting for this by, say, taking a fixed physical density in all three simulations will actually tend to make the slope of the SFR_{ff} vs. M_s curve even steeper, since a higher threshold in code units should be used in Ms24J6, leading to an even smaller measured SFR_{ff} . Thus, this effect cannot account for the fact that we measure a steeper slope than that predicted by KM05.

from ~ 1.6 to a few times t'_{ff} (Larson 1969; Gómez et al. 2007; Galván-Madrid et al. 2007), due to the non-negligible role of the thermal pressure. However, KM05 used t'_{ff} (Krumholz & Tan 2007), so our measured masses are larger than those that would be measured out to t_{ff} by a factor of a few, raising the intercept of our fit with respect to that of KM05.

On the other hand, possible physical effects are: a) the fact discussed in §4 that the clumps in each simulation lack support in comparison with the KM05 model because the motions are not fully random, but instead involve a significant inflow component. b) Most importantly, the mass that appears to be collapsing in our simulations is not that in subsonic, super-Jeans regions, but rather the mass in regions in regions that are supersonic but still gravitationally unstable. This allows for a larger amount of mass involved in the collapse, since in general regions with larger velocities are expected to be larger, and thus more massive. In conclusion, it is not possible to determine whether the differences between the KM05 prediction for SFR_{ff} and our results are significant. However, it is clear that the mechanism of collapse acting in our simulations is different from what they, as well as Padoan (1995) and Vázquez-Semadeni et al. (2003), assumed, since there are no subsonic, super-Jeans structures in our simulations.

6 DISCUSSION AND COMPARISON TO PREVIOUS WORK

6.1 Velocity convergence

Our results have a number of implications for our understanding of the velocity field in MCs and for analytical models of star formation. A first result is that in sub-boxes of the large-scale run (Ms24J6) of the same size as the small-scale run (Ms8J2), the velocity field exhibits a clear trend towards being convergent if the subregion is overdense with respect to the rest of the simulation. This suggests that run Ms8J2, with its zero overall mean divergence, is not representative of the typical region of the same size embedded within a larger medium, since it lacks an expected mean divergence of $\sim -0.6 \text{ km s}^{-1} \text{ pc}^{-1}$, as predicted by eq. (3).

This result also suggests that a significant component of the observed linewidths in MCs and their substructure should be compressive (i.e., conform with the LSI scenario), in agreement with the original suggestion of Goldreich & Kwan (1974). It is even more relevant that this result is observed in numerical simulations of *driven* turbulence (with the driving applied at the large scales and being purely rotational), contrary to the frequent belief that such large-scale inflows occur only in decaying turbulence. It is necessary to stress, however that our analyses cannot distinguish whether the convergent motions in the overdense regions are a cause or a consequence of gravitational contraction. This is beyond the diagnosing capabilities of the studies we have performed.

Dimensionally, the values of the mean divergences we have found for the sub-boxes of our large-scale simulation can be compared to the typical values of the velocity gradients found by Goodman et al. (1993) in dense cores of MCs, which they however interpreted as representative of uniform

rotation. For cores with typical sizes between ~ 0.1 and 1 pc , those authors found velocity gradients ranging between 0.3 and $4 \text{ km s}^{-1} \text{ pc}^{-1}$. Our average value of the velocity divergence for regions of the same size and density as those of run Ms8J2, $\nabla \cdot \mathbf{v} \sim -0.6 \text{ km s}^{-1} \text{ pc}^{-1}$, seems to be on the low side of this distribution, although it may seem reasonable if we consider that only a *fraction* of the kinetic energy should be compressive (i.e., non-rotational) in general. We can also compare with Larson’s (1981) linewidth-size relation, which, for ^{12}CO and ^{13}CO data reads $\Delta v \approx 1 \text{ km s}^{-1} [L/1 \text{ pc}]^{1/2}$ (e.g., Solomon et al. 1987; Heyer & Brunt 2004). Thus, for $L \sim 1 \text{ pc}$, Larson’s relation predicts a velocity dispersion roughly 1.8 times that of our “typical” velocity convergence at the scale of run Ms8J2, given by eq. (3), suggesting that, on average, the velocity dispersion contains comparable amounts of compressive and non-compressive energy. Of course, the fluctuations are large on both our velocity convergence-density relation (eq. 3) and on Larson’s relation, so large deviations from this mean trend can be expected in individual clumps.

Since the compressive part of the velocity works to promote compression, the main implication of our result is that *not all of the non-thermal kinetic energy in clouds and clumps is available for support against gravity*, a fact that has been overlooked by analytic models of star formation from the turbulent conditions in molecular clouds and clumps. In particular, the models by PN02 and KM05 assume that a star-forming core must exceed the thermal Jeans mass in order to collapse but, as shown by Hunter & Fleck (1982), this mass is reduced in the presence of a compressive velocity field. The model by Hennebelle & Chabrier (2008) does consider an additional “support” by the turbulence, but this may again be reduced if the “turbulence” actually contains a significant fraction of inwards motions.

The LSI scenario is naturally motivated by the fact that only compressive motions can produce density fluctuations, while vortical modes are incompressible. Thus, if the density enhancements (clumps) in a flow are produced by turbulent fluctuations, the velocity field within these clumps is likely to still exhibit the signature of the external convergent motions that formed them (Ballesteros-Paredes, Vázquez-Semadeni, & Scalo 1999). This scenario also has the implication that the largest velocity dispersions are expected to occur not in the densest parts of the structures, but at their outskirts, since the densest gas has been shocked and has slowed down (Klessen et al. 2005; Gómez et al. 2007). This effect has been found observationally, albeit with lower velocity dispersion than in the models (see, e.g., André, Basu & Inutsuka 2008, and references therein). Finally, the LSI scenario is also fully consistent with the observation by Heyer & Brunt (2007) that Principal Component Analysis of the velocity field in molecular clouds and their substructure systematically shows the dominance of a whole-cloud dipolar pattern.

At first sight, one could think of two possible ways to avoid the LSI picture. One possibility would occur if the clumps were quasi-static structures in single-phase media confined by ram pressure (Bertoldi & McKee 1992). In this case, the boundaries must be accretion shocks (Folini & Walder 2006; Whitworth et al. 2007; Gómez et al. 2007), so that the mass of the structures must grow over time, possibly eventually becoming strongly self-gravitating

and proceeding to collapse. Thus, even though such clumps can be quasi-static in their central parts, they must be surrounded by an accreting envelope that involves a net convergence of the velocity field (Gómez et al. 2007). The other possibility would occur if the medium, even within MCs, turns out to be thermally bistable (Hennebelle & Inutsuka 2006), in which case the clumps could be hydrostatic objects bound by the thermal pressure of their warm, tenuous environment, as in the classic two-phase model of Field, Goldsmith, & Habing (1969). However, even if molecular clouds are thermally bistable, clumps that are at much higher thermal pressures than their surroundings must be driven either by ram-pressure compressions or by self-gravity (Banerjee et al. 2008). So, there appears to be no escape from the need to have convergent flows involved in the formation and evolution of the densest, star-forming clumps.

6.2 Absence of subsonic, super-Jeans structures

Another result we have obtained is that, in our driven-turbulence simulations, no simultaneously subsonic and super-Jeans structures were found, either before or after self-gravity was turned on. Of course, this result does not rule out the existence of such structures, and in fact subsonic, super-Jeans cores are routinely observed (e.g., Myers 1983; André et al. 2007). Our result may be an artifact of the turbulence being continually driven and/or the absence of magnetic fields and/or the fact that the actual values of α in our simulations are somewhat greater than unity. Nevertheless, our simulations produced abundant collapse, indicating that the formation of simultaneously subsonic and super-Jeans structures (Padoan 1995; Vázquez-Semadeni et al. 2003) is not the only possible route to collapse. Since this notion is at the foundation of models such as those of PN02 and KM05, it is likely that those models may need to be revised to consider the possibility that stars may form via the collapse of larger-scale, supersonic regions, in which the motions are not fully supportive against gravity.

It is also important to reconsider the results of Vázquez-Semadeni et al. (2003) in the light of our present results. In that paper it was shown that there exists a correlation between the sonic scale of the turbulence and the SFE, so that, as the sonic scale becomes smaller (at constant J), the SFE decreases. This was interpreted as indirect evidence that the available mass for collapse decreased as the sonic scale became smaller, and therefore that the collapsed objects indeed originated from subsonic, super-Jeans structures. However, our finding that there exist alternative routes to collapse that are not based on the formation of subsonic, super-Jeans structures suggests that the correlation found by Vázquez-Semadeni et al. (2003) may be simply indicative of a general scaling of both the SFE and the sonic scale with rms Mach number, but not that the fraction of mass in subsonic, super-Jeans structures directly measures the mass that is on route to collapse at any given time.

6.3 Role of gravity in the formation of Jeans-unstable structures and the density PDF

Our simulations also suggest that self-gravity is not only involved in the *capture* of turbulent density fluctuations to make them collapse, but also in the *production* of collapsing objects, as shown by the distortion of the density PDF and by the increase of the fraction of self-gravitating regions at small scales in the presence of self-gravity. In this sense, these results may represent the driven-turbulence counterpart of the results by Clark & Bonnell (2005), who concluded from decaying turbulence simulations that the turbulence does not directly produce the collapse of clumps by making them reach their own Jeans mass, but rather just produces the seeds for subsequent gravitational fragmentation of the large-scale gravitationally unstable structures. In our driven case, it appears that turbulence alone produces only a few super-Jeans structures, while, in the presence of self-gravity, super-Jeans objects are much more readily produced.

This result is likely to have an implication for the PN02 model. This model assumes that turbulence alone is responsible for the formation of the cores, with gravity only playing a role if they become Jeans unstable and collapse. Our results suggest instead that turbulence alone is insufficient for producing a hierarchy of structures whose mean densities scale with size in a Larson (1981)-like way (recall our simulations are constructed to have mean densities inversely proportional to their sizes, but turbulence alone appears incapable of producing regions like run Ms8J2 within run Ms24J6). Turbulence must be considered in conjunction with self-gravity for the production of the denser structures.

This fact is also likely to have an implication for the interpretation of the recent findings by Joung & Mac Low (2006). These authors concluded from non-self-gravitating simulations of the supernova-driven ISM with a fixed imposed supernova rate, that this driving alone is insufficient to sustain itself, as it does not deposit a sufficiently large amount of mass in Jeans-unstable regions to be consistent with the imposed supernova rate. Our result that gravity participates in the *formation* of Jeans-unstable regions suggests that the discrepancy between the applied supernova rate and the rate of production of Jeans-unstable regions in their simulations they reported (roughly an order of magnitude) may actually be an upper limit, so that supernova driving may be more efficient in driving secondary star formation than they concluded.

Finally, the fact that the density PDF develops a high-density tail in the presence of self-gravity also has implications. Several models and calculations (e.g., Elmegreen 2002; Padoan & Nordlund 2002; Krumholz & McKee 2005) rely on this distribution, and it is necessary to assess the degree to which such a deviation may alter the results of these models.

6.4 Star formation rate per free-fall time

We have also measured the SFR_{ff} in our three simulations, all of which have turbulent driving applied at the largest scales in each simulation, and approximately the same virial parameter α , thus matching the assumption made by KM05

to derive their equation (30) (eq. [5] in the present paper) that star-forming clouds and clumps are all nearly virialized, with $\alpha \sim 1$. We found the SFR_{ff} s in our simulations to be marginally consistent (i.e., within the range allowed by our uncertainties) with the prediction of the model. This is not surprising, since our suite of simulations was specifically designed to satisfy the $\alpha \sim 1$ assumption of KM05. Note however that, in spite of this specific design of the simulations, at face value the slope of the SFR_{ff} vs. M_s we find is larger than the prediction by KM05. This may be a reflection of our result that the sub-boxes of the large-scale simulation Ms24J6 with the same size and mean density as the small-scale simulation Ms8J2 differed from it in that they contain a non-zero mean convergence of the velocity field. This result contradicts the *hypothesis* of the KM05 model (and many others, e.g., Elmegreen 2002; McKee & Tan 2003; Mac Low & Klessen 2004; Hennebelle & Chabrier 2008) that the turbulence at every scale is completely random, and therefore acts as an isotropic pressure that provides support against the self-gravity of the entire structure. If in reality clouds and clumps contain a significant amount of kinetic energy in convergent motions that do not oppose gravity, the dependence of the SFE on M_s at $\alpha \sim 1$ might actually be somewhat steeper than the prediction by KM05. This in fact may be the reason why our simulations give a mean larger exponent in the relation between SFR_{ff} and M_s , since, even though each one of our simulations was constructed as to have a random global turbulent velocity field, the clumps formed self-consistently within them do not, on average.

A final note of caution, however, is that our results have been obtained in the simplest possible numerical setup, namely non-magnetic, isothermal media without stellar feedback, and as such, cannot be considered definitive. We plan to investigate thermally bistable, magnetized media with stellar feedback in future works.

ACKNOWLEDGMENTS

We thank Patrick Hennebelle for a critical reading of an earlier version of the manuscript and useful comments, and an anonymous referee for a thoughtful and thorough report that much helped in improving the paper. The numerical simulations were performed on the Cluster Platform 4000 (KanBalam) of DGSCA, UNAM. This work has received financial support from grant U47366-F (CONACYT) to E.V.-S., grants IN111606 and IN 117708 to R.F.G., IN110606 to J.B.-P., and 111006-3 to A.G. J.K. was supported in part by KOSEF through the Astrophysical Research Center for the Structure and Evolution of Cosmos and the grant of the basic research program R01-2007-000-20196-0.

REFERENCES

- André, Ph., Belloche, A., Motte, F., & Peretto, N. 2007, *A&A*, 472, 519
- André, Ph., Basu, S., & Inutsuka, S.-I. 2008, in *Structure Formation in the Universe: Galaxies, Stars, Planets*, ed. G. Chabrier (Cambridge: Cambridge University Press), in press (arXiv:0801.4210)
- Arons, J., & Max, C. E. 1975, *ApJ*, 196, L77
- Audit, E. & Hennebelle, P. 2005, *A&A* 433, 1
- Ballesteros-Paredes, J. 2006, *MNRAS*, 372, 443
- Ballesteros-Paredes, J., & Hartmann, L. 2007, *RMAA*, 43, 123
- Ballesteros-Paredes, J., Vázquez-Semadeni, E., & Scalo, J. 1999, *ApJ*, 515, 286
- Banerjee, R., Vázquez-Semadeni, E., Hennebelle, P., & Klessen, R. S. 2008, in preparation
- Bate, M. R., Bonnell, I. A., & Bromm, V. 2003, *MNRAS* 336, 705
- Bertoldi, F. & McKee, C. F. 1992, *ApJ* 395, 140
- Bonnell, I. A., Bate, M. R. 2006, *MNRAS*, 370, 488
- Brunt, C. M. 2002, *ApJ* 583, 280
- Clark, P. C., & Bonnell, I. A. 2005, *MNRAS*, 361, 2
- Cho, J., Lazarian, A., & Vishniac, E. T. 2002, *ApJ*, 564, 291
- Dib, S., & Burkert, A. 2005, *ApJ*, 630, 238
- Dib, S., Kim, J., Vázquez-Semadeni, E., Burkert, A., & Shadmehri, M. 2007, *ApJ*, 661, 262
- Elmegreen, B. G. 2002, *ApJ*, 577, 206
- Elmegreen, B. G. 2007, *ApJ*, 668, 1064
- Field, G. B., Goldsmith, D. W., & Habing, H. J. 1969, *ApJ*, 155, L149
- Field, G. B., Blackman, E. G., Keto, E. R. 2008, *MNRAS*, 385, 181
- Folini, D. & Waldr, R. 2006, *A&A*, 459, 1
- Franco, J. Shore, S. N., & Tenorio-Tagle, G. 1994, *ApJ* 436, 795
- Frisch, U. 1995, *Turbulence. The legacy of A.N. Kolmogorov* (Cambridge: Cambridge University Press)
- Galván-Madrid, R., Vázquez-Semadeni, E., Kim, J., & Ballesteros-Paredes, J. 2007, *ApJ*, 670, 480
- Goldreich, P., & Kwan, J. 1974, *ApJ* 189, 441
- Gómez, G. C., Vázquez-Semadeni, E., Shadmehri, M., & Ballesteros-Paredes, J. 2007, *ApJ*, 669, 1042
- Goodman, A. A., Benson, P. J., Fuller, G. A., & Myers, P. C. 1993, *ApJ* 406, 528
- Hartmann, L., Ballesteros-Paredes, J., & Bergin, E. A. 2001, *ApJ*, 562, 852
- Hartmann, L. & Burkert, A. 2007, *ApJ*, 654, 988
- Heitsch, F., Burkert, A., Hartmann, L., Slyz, A. D. & Devriendt, J. E. G. 2005, *ApJ* 633, L113
- Heitsch, F., Slyz, A., Devriendt, J., Hartmann, L., & Burkert, A. 2006, *ApJ* 648, 1052
- Heitsch, F., Mac Low, M. M., & Klessen, R. S. 2001, *ApJ*, 547, 280
- Hennebelle, P., & Chabrier, G. 2008, *ApJ*, in press (arXiv:0805.0691)
- Hennebelle, P., & Inutsuka, S.-I. 2006, *ApJ*, 647, 404
- Hennebelle, P., Mac Low, M.-M., & Vázquez-Semadeni 2007, in *Structure Formation in the Universe: Galaxies, Stars, Planets*, ed. G. Chabrier (Cambridge: Cambridge University Press), in press (arXiv:0711.2417)
- Heyer, M., & Brunt, C. 2004, *ApJ*, 615, L45
- Heyer, M., & Brunt, C. 2007, in *Triggered Star Formation in a Turbulent ISM*, eds. B. G. Elmegreen & J. Palouš (Cambridge: Cambridge University Press), 9
- Hunter, J. H., Jr., & Fleck, R. C., Jr. 1982, *ApJ*, 256, 505
- Joung, M. K. R., & Mac Low, M.-M. 2006, *ApJ*, 653, 1266
- Kim, J., Ryu, D., Jones, T. W., & Hong, S. S. 1999, *ApJ*, 514, 506

- Kim, W.-T., & Ostriker, E. C. 2006, *ApJ* 646, 213
- Klessen, R. S., 2000, *ApJ*, 535, 869
- Klessen, R. S., Heitsch, F., & MacLow, M. M. 2000, *ApJ*, 535, 887
- Klessen, R. S., Ballesteros-Paredes, J., Vázquez-Semadeni, E., & Durán-Rojas, C. 2005, *ApJ* 620, 786
- Koyama, H. & Inutsuka, S.-I. 2002, *ApJ*, 564, L97
- Krumholz, M. R., Matzner, C. D., & McKee, C. F. 2006, *ApJ*, 653, 361
- Krumholz, M. R., & McKee, C. F. 2005, *ApJ*, 630, 250
- Krumholz, M. R., & Tan, J. C. 2007, *ApJ*, 654, 304
- Lada, C. J., & Lada, E. A. 2003, *ARA&A*, 41, 57
- Larson, R. B. 1969, *MNRAS*, 145, 271
- Larson, R. B. 1981, *MNRAS*, 194, 809
- Larson, R. B. 1987, in *Starbursts and galaxy evolution*, ed. T.X. Thuan, T. Montmerle, J. Tran Thanh Van (Gif-sur-Yvette: Editions Frontières), 467
- Leisawitz, D., Bash, F. N., & Thaddeus, P. 1989, *ApJS*, 70, 731
- Li, Y., Mac Low, M.-M., & Klessen, R. S. 2005, *ApJ*, 620, L19
- Mac Low, M.-M. 1999, *ApJ*, 524, 169
- Mac Low, M.-M., & Klessen, R. S. 2004, *Rev. Mod. Phys.*, 76, 125
- Matzner, C. D., & McKee, C. F. 2000, *ApJ*, 545, 364
- McKee, C. F. 1989, *ApJ*, 345, 782
- McKee, C. F., Ostriker, E. C. 2007, *ARA&A*, 45, 565
- McKee, C. F., Tan, J. C. 2003, *ApJ*, 585, 850
- Mouschovias, T. C. 1976, *ApJ* 206, 753
- Myers, P. C. 1983, *ApJ* 270, 105
- Nakamura, F., & Li, Z.-Y. 2007, *ApJ*, 395, 412
- Nordlund, Å., & Padoan, P. 1999, in *Interstellar Turbulence*, ed. J. Franco, and A. Carramiñana (Cambridge: Cambridge University Press), 218
- Norman, C. & Silk, J. 1980, *ApJ*, 238, 158
- Ossenkopf, V., & Mac Low, M.-M. 2002, *A&A*, 390, 307
- Padoan, P. 1995, *MNRAS*, 277, 377
- Padoan, P. & Nordlund 1999, *ApJ*, 526, 279
- Padoan, P. & Nordlund 2002, *ApJ*, 576, 870
- Passot, T., & Vázquez-Semadeni, E. 1998, *Phys. Rev. E.*, 58, 4501
- Peretto, N., Hennebelle, P., Andr, P. 2007, *A&A*, 464, 983
- Sasao, T. 1973, *PASJ*, 25, 1
- Shu, F. H., Adams, F. C., & Lizano, S. 1987, *ARA&A*, 25, 23
- Solomon, P. M., Rivolo, A. R., Barrett, J., & Yahil, A. 1987, *ApJ*, 319, 730
- Stone, J. M., Ostriker, E. C., & Gammie, C. F. 1998, *ApJ*, 508, L99
- Vázquez-Semadeni, E., 1994, *ApJ*, 423, 681
- Vázquez-Semadeni, E., Ballesteros-Paredes, J. & Klessen, R. S. 2003, *ApJ*, 585, L131
- Vázquez-Semadeni, E., Kim, J., & Ballesteros-Paredes, J. 2005, *ApJ*, 630, L49
- Vázquez-Semadeni, E., Kim, J., Shadmehri, M. & Ballesteros-Paredes, J. 2005, *ApJ*, 618, 344
- Vázquez-Semadeni, E., Ryu, D., Passot, T., González, R. F., & Gazol, A., 2006, *ApJ*, 643, 245
- Vázquez-Semadeni, E., Gómez, G. C., Jappsen, A. K., Ballesteros-Paredes, J., González, R. F., & Klessen, R. S. 2007, *ApJ*, 657, 870
- Vázquez-Semadeni, E., & Passot, T. 1999, in *Interstellar Turbulence*, ed. J. Franco and A. Carramiñana (Cambridge: Cambridge University Press), 223
- Whitworth, A. 1979, *MNRAS*, 186, 59
- Whitworth, A., Bate, M. R., Nordlund, ., Reipurth, B., & Zinnecker, H., in *Protostars and Planets V*, ed. B. Reipurth, D. Jewitt, and K. Keil (Tucson: University of Arizona Press), 459
- Zuckerman, B., & Evans, N. J. 1974, *ApJ*, 192, L149
- Zuckerman, B. & Palmer, P. 1974, *ARA&A*, 12, 279

This paper has been typeset from a $\text{T}_{\text{E}}\text{X}/\text{L}^{\text{A}}\text{T}_{\text{E}}\text{X}$ file prepared by the author.